

# Linking plankton size spectra and community composition to carbon export and its efficiency

Camila Serra-Pompei<sup>1,3\*</sup>, Ben A. Ward<sup>2</sup>, Jérôme Pinti<sup>1,4</sup>, André W. Visser<sup>1</sup>,  
Thomas Kiørboe<sup>1</sup>, Ken H. Andersen<sup>1</sup>

<sup>1</sup>Centre for Ocean Life, Technical University of Denmark, DTU Aqua, Kemitorvet B201, Kongens Lyngby 2800, Denmark.

<sup>2</sup>Ocean and Earth Science, University of Southampton, Southampton, UK.

<sup>3</sup>Department of Earth, Atmospheric and Planetary Sciences, Massachusetts Institute of Technology, Cambridge, MA 02139, USA.

<sup>4</sup>College of Earth, Ocean and Environment, University of Delaware, Lewes, DE 19958, USA.

## Key Points:

- We use a global mechanistic size-spectrum model to investigate the relation between particulate export and plankton community metrics.
- We find a good correlation between export efficiency and the exponent of the size spectrum.
- Total carbon export correlated well with copepod biomass and trophic level of active copepods in the model.

---

\*Current address, Department of Earth, Atmospheric and Planetary Sciences, Massachusetts Institute of Technology, Cambridge, MA 02139, USA

Corresponding author: Camila Serra-Pompei, [camsp@mit.edu](mailto:camsp@mit.edu)

18 **Abstract**

19 The magnitude and efficiency of particulate carbon export from the ocean surface de-  
20 pends not only on net primary production (NPP) but also on how carbon is consumed,  
21 respired, and repackaged by organisms. We contend that several of these processes can  
22 be captured by the size spectrum of the plankton community. However, most global mod-  
23 els have relatively simple food-web structures that are unable to generate plankton size-  
24 spectra. Moreover, the life-cycles of multicellular zooplankton are typically not resolved,  
25 restricting the ability of models to represent time-lags that are known to impact carbon  
26 export and its efficiency (pe-ratio). Here, we use a global mechanistic size-spectrum model  
27 of the marine plankton community to investigate how particulate export and pe-ratio  
28 relate to the community size spectrum, community composition, and time-lags between  
29 predators and prey. The model generates emergent food-webs with associated size dis-  
30 tributions for organisms and detrital particles. To resolve time-lags between phytoplank-  
31 ton and zooplankton, we implement the life-cycle of multicellular zooplankton (here rep-  
32 resented by copepods). The simulation successfully captures observed patterns in biomass  
33 and energy fluxes across regions. We find that carbon export correlates best with cope-  
34 pod biomass and trophic level, whereas the pe-ratio correlates best with the exponent  
35 of the size spectrum and sea surface temperature (SST). Community metrics performed  
36 better than NPP or SST for both deep export and pe-ratio. Time-lags between phyto-  
37 plankton and copepods did not strongly affect export or pe-ratio. We conclude by dis-  
38 cussing how can we reconcile size-spectrum theory with field sampling.

39 **Plain Language Summary**

40 Plankton are tiny but extremely abundant aquatic organisms. Plankton lock CO<sub>2</sub>  
41 away from the atmosphere as they sink to the deep ocean, where carbon can be stored  
42 for hundreds of years. However, how much carbon is locked away and for how long de-  
43 pends on how organisms eat, defecate, and respire. We argue that these processes are  
44 reflected in the size composition of the plankton community. The size composition shows  
45 a clear relationship between the number of organisms and their body-size. The steep-  
46 ness of this “size-abundance relationship” describes the balance between small vs. large  
47 organisms, and has been argued to reflect how energy is transferred from small to large  
48 organisms. Since large organisms create fast-sinking particles, the size-abundance rela-  
49 tionship could be used to estimate how much carbon is being stored in the deep ocean.  
50 Here we use a computer simulation of the global plankton community to investigate how  
51 the removal of carbon relates to the plankton community and the steepness of the size-  
52 abundance relationship. The model successfully captures patterns observed in nature.  
53 We found that the size-abundance relationship, together with the quantity of large zoo-  
54 plankton better explained carbon export than other measures typically used, such as pho-  
55 tosynthesis and temperature.

56 **1 Introduction**

57 Plankton contribute to the removal of atmospheric CO<sub>2</sub> by photosynthesizing in  
58 the surface ocean and sinking into the deep ocean, where remineralized carbon may re-  
59 main sequestered for hundreds of years (Longhurst & Harrison, 1989; Ducklow et al., 2001).  
60 The amount of carbon exported and carbon export efficiency emerge from intricate pro-  
61 cesses that result in either carbon being respired in the surface ocean – and therefore not  
62 sequestered – or exported and respired in the deep ocean. Where and how much carbon  
63 is respired depends on the community composition and interactions between organisms  
64 who eat, respire, and excrete this carbon several times as energy flows across the food-  
65 web. However, due to the large amount of players and processes that alter carbon ex-  
66 port, global estimates of the flux out of the euphotic zone are highly uncertain, ranging

67 from  $\approx 3$  to  $12 \text{ PgC year}^{-1}$  (Dunne et al., 2005; S. Henson et al., 2011; DeVries & Weber, 2017).

69 Community composition and interactions between organisms drive carbon export  
70 and its efficiency (Ducklow et al., 2001; S. Henson et al., 2019). In general, food-webs  
71 that are dominated by large organisms are expected to efficiently export large amounts  
72 of carbon (Wassmann, 1997; Stamieszkin et al., 2015). This is because large organisms  
73 produce fast-sinking particles (Small et al., 1979). These food-webs tend to be short, where  
74 NPP efficiently reaches large organisms (Wassmann, 1997). Conversely, food-webs dom-  
75 inated by small organisms tend to be long, with many trophic transfers. Each trophic  
76 transfer results in respiration losses, and therefore long food-webs with many trophic lev-  
77 els result in carbon being exported inefficiently (Wassmann, 1997).

78 Time-lags between phytoplankton and zooplankton are another factor that has been  
79 suggested to affect carbon export (Parsons, 1988; S. A. Henson et al., 2015; S. Henson  
80 et al., 2019). These time-lags result from the slower demographic response of multicel-  
81 lular zooplankton (e.g. copepods) relative to phytoplankton growth rate. Multicellular  
82 zooplankton need to grow in body size before being able to reproduce. This ontogenetic  
83 growth prevents multicellular zooplankton populations to grow as fast as phytoplank-  
84 ton that grow by cell division. In contrast, unicellular zooplankton (that also grow by  
85 cell division) are able to tightly follow phytoplankton dynamics. Grazing by unicellu-  
86 lar zooplankton often results in low export efficiencies, as they contribute to long food-  
87 webs dominated by small organisms (McNair et al., 2021), where most carbon is resired  
88 in the surface ocean. Hence, differences in life-history strategies between prey and pred-  
89 tors can alter the amount of carbon exported.

90 Food-web structure, organismal size distributions, and the life cycle of organisms  
91 are therefore important factors contributing to carbon export and its efficiency. How-  
92 ever, most models that simulate carbon export have similar simple food-web configura-  
93 tions. These food-web configurations tend to resolve a small and a large group of each  
94 component of the ecosystem: phytoplankton, zooplankton, and detritus (e.g. Laws et  
95 al., 2000; Siegel et al., 2014; S. A. Henson et al., 2015; DeVries & Weber, 2017; Bisson  
96 et al., 2020). These food-webs have fixed interactions, where the small/large zooplank-  
97 ton eats the small/large phytoplankton (and perhaps the large zooplankton also eats the  
98 small zooplankton). Yet, marine systems tend to form size-spectra with complex inter-  
99 actions (Sprules & Munawar, 1986; Sprules & Barth, 2016; Hartvig et al., 2011). Organ-  
100 isms of the same size can occupy different trophic levels, or the same organism can be  
101 at a different trophic level depending on the environmental conditions. In addition, in  
102 these models, no life cycle differences are made between zooplankton groups, prevent-  
103 ing time-lags between prey and predators. Simple food-web configurations are convenient  
104 to understand some of the main interactions, but also miss several of the factors men-  
105 tioned above. Hence, incorporating flexible food-web configurations, life histories, and  
106 size-spectra in ecosystem models might help identify new processes driving carbon ex-  
107 port and its efficiency.

108 A major factor shaping marine food-webs is body-size (Hartvig et al., 2011; An-  
109 dersen et al., 2016). Predator-prey interactions are size-dependent, where typically large  
110 eats small, and metabolic processes follow allometric relationships (Kiørboe & Hirst, 2014).  
111 In marine systems, the combination of these processes results in body-mass normalized  
112 size-spectra closely resembling power-law functions ( $B = \kappa m^\lambda$ ), with varying coefficient  
113 ( $\kappa$ ) and exponent ( $\lambda$ ) (Sprules & Barth, 2016; Andersen, 2019). Differences in the co-  
114 efficient indicate differences in the bulk biomass, whereas differences in the exponent show  
115 changes in the balance of small vs. large organisms, reflecting how efficiently energy and  
116 biomass reach larger organisms (Andersen et al., 2009). Among the emergent size spec-  
117 tra, low exponents (steeper spectra) indicate that energy is inefficiently channeled to-  
118 wards large organisms (inefficient food-webs), while communities with high exponents  
119 (flatter spectra) efficiently channel NPP to large organisms (efficient food-webs). The

120 exponent of the size spectrum is thus a good indicator of food-web efficiency, and is therefore  
121 a potentially good indicator of carbon export and its efficiency.

122 Here we seek to understand how carbon export and its efficiency relate to community  
123 composition, food-web structure, size spectra, and trophic interactions between prey  
124 and predators. To do so, we use a mechanistic model of the planktonic community cou-  
125 pled to a 3D representation of a global ocean circulation model. We use the Nutrient-  
126 Unicellular-Multicellular (NUM) size-spectrum model of the planktonic community (Serra-  
127 Pompei et al., 2020). This framework is built upon the main processes at the individ-  
128 ual level: physiology and prey size preference and encounter. The life cycle of multicel-  
129 lular zooplankton is also resolved, differentiating them from unicellular zooplankton. The  
130 model yields size spectra of plankton and detrital particles, which are important to de-  
131 termine particle sinking rates. Overall, food-web structure and the resulting particle ex-  
132 port are emergent properties from biological interactions between organisms and the en-  
133 vironment.

## 134 2 Methods

135 The NUM framework is a mechanistic size- and trait-based model of the planktonic  
136 community (Serra-Pompei et al., 2020). The original model resolves the size distribu-  
137 tion of unicellular protists (autotrophic, mixotrophic, heterotrophic), the copepod com-  
138 munity, copepod fecal pellets, and one pool of nitrogen. Here, the model has been ex-  
139 tended to account for the size-distribution of dead cells and dead copepods, together re-  
140 ferred to as deadfalls. The ecological model is embedded in a 3D transport matrix that  
141 represents advection and mixing of the ocean physical environment (Khatiwala, 2007).  
142 Here, we briefly explain the model and illustrate the main concepts (Fig. 1). A detailed  
143 explanation of the model and its equations can be found in the supplementary material  
144 and in (Serra-Pompei et al., 2020).

### 145 2.1 Ecological model

146 The model is mechanistic, where we use empirically demonstrated mechanisms at  
147 the individual level to scale to the population, community and ecosystem levels. The model  
148 generates a community of protists, copepods, fecal pellets, and deadfalls (Fig. 1c). To  
149 obtain the community size-spectrum, the model simulates several size-classes of each com-  
150 partment (Fig. 1b). Protists are discretized in populations characterised by the organ-  
151 ism's size. Copepods also have several populations, each characterised by the adult body-  
152 mass and feeding mode. Each copepod population grows in body-size as they mature  
153 from nauplii to adults that can reproduce (Fig. 1b). The growth from nauplii to adult-  
154 hood results in changes of up to two orders of magnitude in body mass. Copepods pro-  
155 duce fecal pellets that are proportional to the organism size. Finally, both protists that  
156 die through viral lysis and copepods that die through non-consumptive mortality result  
157 in deadfalls of sizes that depend on the size of the producer. Therefore, size is the main  
158 trait describing organisms and particles, and physiological rates, predator-prey interac-  
159 tions, and sinking rates of particles are all size-dependent.

160 We consider different protist trophic strategies and copepod feeding modes. Here,  
161 protists are mixotrophic “generalists” (Fig. 1a); i.e. they can simultaneously photosyn-  
162 thesize, take up dissolved nutrients, and eat other organisms. Size resolves the emergence  
163 of the distinct trophic strategies across the protist size spectrum (Chakraborty et al., 2017).  
164 For example, since the smallest protists don't have prey to eat and have a competitive  
165 advantage in nitrogen uptake, they will mainly be autotrophs. On the other hand, there  
166 is more prey available for large protists, and therefore they will tend to be heterotrophs.  
167 Intermediate sized protists will tend to be mixotrophs. Still, environmental conditions  
168 and prey availability will define the best trophic strategy for each size-class. As for cope-  
169 pods, we make a distinction between “active” and “passive” feeding modes. Active cope-

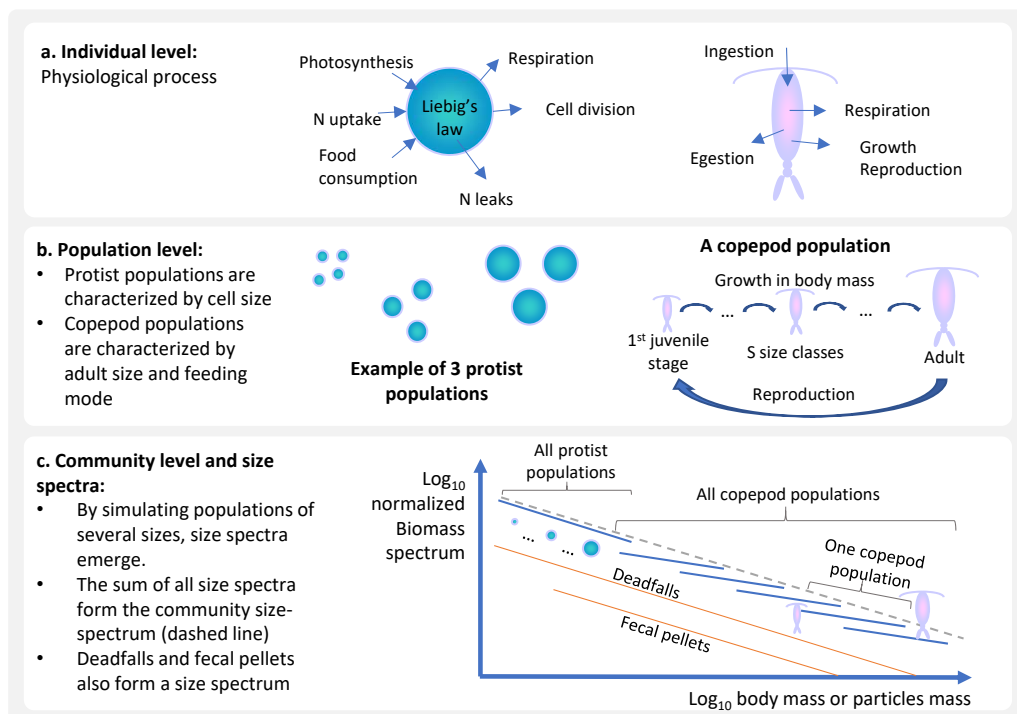


**Figure 1.** Diagram of the ecological model. (a) Community level processes are scaled from rates at the individual level, which depend on resources and prey availability as well as temperature and organism size. (b) A population is the combination of organisms that have the same trait combinations, here cell mass for protists and adult body mass and feeding mode (active vs. passive) for copepods (b). Finally, (c) the combination of all populations results in community-level processes and the emergence of size-spectra.

170 pods include cruising copepods and feeding-current feeders that encompass most calanoid  
 171 copepods. Passive feeding copepods are ambush “sit-and-wait” feeders that include some  
 172 calanoids and most cyclopoids. Active feeding copepods constantly search for food, have  
 173 high metabolic expenditures, and are more easily detected by predators. Conversely, pas-  
 174 sive feeders avoid predation by waiting for their prey to come, resulting in a lower avail-  
 175 ability of prey. These two feeding modes include the feeding strategies of most pelagic  
 176 copepods.

177 Organisms in the model interact through competition and predation (Fig. 1). Cope-  
 178 pods feed on protists, on other copepods, and on deadfalls and fecal pellets. Protists feed  
 179 on other protists, but also have the ability to photosynthesise and take up dissolved ni-  
 180 trogen. Food that is not assimilated by copepods is egested as fecal pellets. The dead  
 181 cells/bodies of organisms that die through viral lysis or other background mortality en-  
 182 ter the deadfalls compartment. Deadfalls are remineralized and can be eaten by cope-  
 183 pods. The sinking rate of fecal pellets and deadfalls is size-dependent. Overall, rather  
 184 than being prescribed, the food-web configuration and resulting community trait-composition  
 185 emerge from the environmental forcing (nitrogen, light, temperature), and the interac-  
 186 tions of competition and predation.

187 **2.2 Biomass spectrum**

188 From the biomass in each size-class we obtain a size distribution of the biomass.  
189 The normalized biomass spectrum results from dividing the biomass in each size range  
190 by the size-range itself. For example, the size spectrum of protists is  $P_{k,\text{spec}} = P_k / \Delta_P$ ,  
191 and thus the unit of the biomass spectrum becomes  $\text{mgC m}^{-3} \text{ }\mu\text{gC}^{-1}$  (where  $\text{mgC m}^{-3}$   
192 corresponds to the biomass concentration in the water and  $\text{ }\mu\text{gC}^{-1}$  to the bin width of  
193 the body-size range). The community size-spectrum is the sum of all the size-spectra.  
194 This normalization allows comparison between compartments, even when bin-sizes dif-  
195 fer (see Sprules & Barth, 2016 and chapter 2 of Andersen, 2019 for more explanations  
196 regarding size-spectra conversions).

197 **2.3 Ocean circulation and environmental forcing**

198 The NUM framework is embedded within a representation of the global ocean cir-  
199 culation, using the “transport matrix method” (Khatiwala et al., 2005; Khatiwala, 2007).  
200 The transport matrix is derived from a coarse resolution ( $2.8^\circ \times 2.8^\circ$ , 15 vertical lev-  
201 els), monthly-averaged simulation of the MITgcm ([http://kelvin.earth.ox.ac.uk/  
202 spk/Research/TMM/TransportMatrixConfigs](http://kelvin.earth.ox.ac.uk/spk/Research/TMM/TransportMatrixConfigs), as used in Dutkiewicz, Follows, & Parekh,  
203 2005). The coarse resolution results in the euphotic zone being resolved in only two or  
204 three layers of the transport matrix. The temperature forcing is monthly averaged. Ir-  
205 radiance at the ocean surface was taken from [http://sites.science.oregonstate.edu/  
206 ocean.productivity/index.php](http://sites.science.oregonstate.edu/ocean.productivity/index.php). The data was afterwards interpolated to fit the grid  
207 of the transport matrix.

208 **2.4 Carbon export and carbon export efficiency (pe-ratio)**

209 The pe-ratio is defined as the fraction of depth-integrated NPP exported as sink-  
210 ing particles at a given depth horizon. For both carbon export and pe-ratio, the depth  
211 horizons used in this study are 120 m and 1080 m, which are the bottom of the second  
212 and the seventh layer of the transport matrix, respectively. We consider the annual and  
213 seasonal pe-ratio. The annual pe-ratio is the ratio between NPP and export flux, both  
214 integrated over a year. The seasonal pe-ratio is the daily particle flux divided by the two  
215 weeks averaged NPP prior to export.

216 **2.5 Numerics**

217 The model configuration is flexible and any reasonable number of state variables  
218 can be implemented. Here, we use 14 protists size-classes (ranging from  $10^{-7} \text{ }\mu\text{gC}$  to  $10^{-1.5} \text{ }\mu\text{gC}$   
219 per cell), and 8 copepod populations (6 populations of active feeding copepods and 2 pop-  
220ulations of passive feeding copepods). Copepods range from  $10^{-3} \text{ }\mu\text{gC}$  for the smallest  
221 nauplii to  $10^4 \text{ }\mu\text{gC}$  for the largest adult copepod. Each copepod population is divided  
222 into 5 size-classes going from nauplii to adults. There are 8 size classes of fecal pellets  
223 and 8 size-classes of deadfalls. There is one pool of dissolved nitrogen. The model was  
224 implemented in MATLAB and run for 15 years. In this run-time, the internal nutrient  
225 dynamics does not reach equilibrium. This would need much longer, unaffordable run  
226 times. To compensate for this, we initiate the nitrogen concentration with nitrate data  
227 from the World Ocean Atlas. By the end of the simulation, most model compartments  
228 reach equilibrium, yet a small drift is present due to the internal nutrient dynamics. The  
229 code can be found in the following GitHub repository [https://github.com/cam-sp/  
230 NUMmodel\\_global.git](https://github.com/cam-sp/NUMmodel_global.git).

231 **2.6 Model testing**

Outputs of the model are compared with field data extracted from the literature.  
Protists biomass is compared with nano- and microplankton data from the upper 50 m

of the water column from three Atlantic Meridional Transects (AMT 12-14, in summer and autumn, San Martin et al. (2006)). Copepod biomass is compared with data from the AMT 13 transect (López & Anadón, 2008). López and Anadón (2008) used a small mesh size and therefore included the smaller size range, which is often omitted in other studies. To calculate the copepod biomass we multiplied the average copepod body-mass by the abundance within each size-range of the study. Exponents of the size spectrum can also be found in San Martin et al. (2006), where they fitted a size-spectrum to nano- and micro-plankton together with mesozooplankton data. To compare net primary production (NPP) we use the data-set collected in Saba et al. (2011), where NPP field data were collected from different campaigns. We show the root mean square difference (RMSD) of NPP for each region to compare with the values obtained in Saba et al. (2011), where RMSD is:

$$RMSD = \left( \frac{1}{N} \sum_{i=1}^N [\log_{10}(NPP_m) - \log_{10}(NPP_d)]^2 \right)^{1/2},$$

where  $N$  is the number of data points,  $NPP_m$  the modeled NPP, and  $NPP_d$  the data values.

For particle export, we use the data compiled in Le Moigne et al. (2013) and extended in S. Henson et al. (2019). In this data-set, the particle export is estimated between 100-200 m depth by the  $^{234}\text{Th}$  technique. Data points of export that fell within the same bin and day of the transport matrix were averaged, and the variability was shown with error bars in the figure. The same procedure was done for the NPP data. Finally, we do not compare modelled pe-ratios with the ones derived in other studies. In other studies pe-ratios are often obtained by using NPP models (from remote sensing) and differences might emerge due to model differences. We therefore stick to validate NPP and export separately without checking pe-ratios from other studies.

### 3 Results

We start by describing the general trends of biomass and energy fluxes in the food-web while comparing them with data. Next, we investigate the drivers of food-web configurations and associated particle export and pe-ratio. All the fluxes discussed are yearly-integrated, except in the last section (3.6) where we consider seasonality.

#### 3.1 Biomass

Protist and copepod biomass follow the same global trend (Fig. 2): high in temperate and sub-polar regions, and lowest in oligotrophic gyres. Compared with latitudinal field-data of nano- and microplankton biomass (Fig. 3), the model falls within observed biomass ranges in the AMT 12 transect (Fig. 3a), and in the northern hemisphere of the AMT 13 transect (Fig. 3b). However, in the latter transect, the model overestimates biomass in the southern hemisphere. This overestimation is probably due to the lack of iron limitation in the model. The model also overestimates protist biomass in the AMT 14 transect despite following well the trend (Fig. 3c). However, the biomass data from this transect is much lower than in the other two transects. Overall, despite the overestimation in some regions, modeled protist biomass follows well the general trend and magnitude of the data.

Copepod biomass trends match well the data from the AMT transect (Fig. 4), despite an overestimation between latitudes -30 and -10 (stations 22 to 18). The latter follow the protist biomass trend that was also overestimated in those regions during October. Relative copepod biomass within body-size ranges is somewhat constant across latitudes, with a dominance of small copepods in most regions (Fig. 4). The model simulates more small copepods than observed. Nevertheless, large copepods are present in most regions, including low productive regions, both in the data and the model.

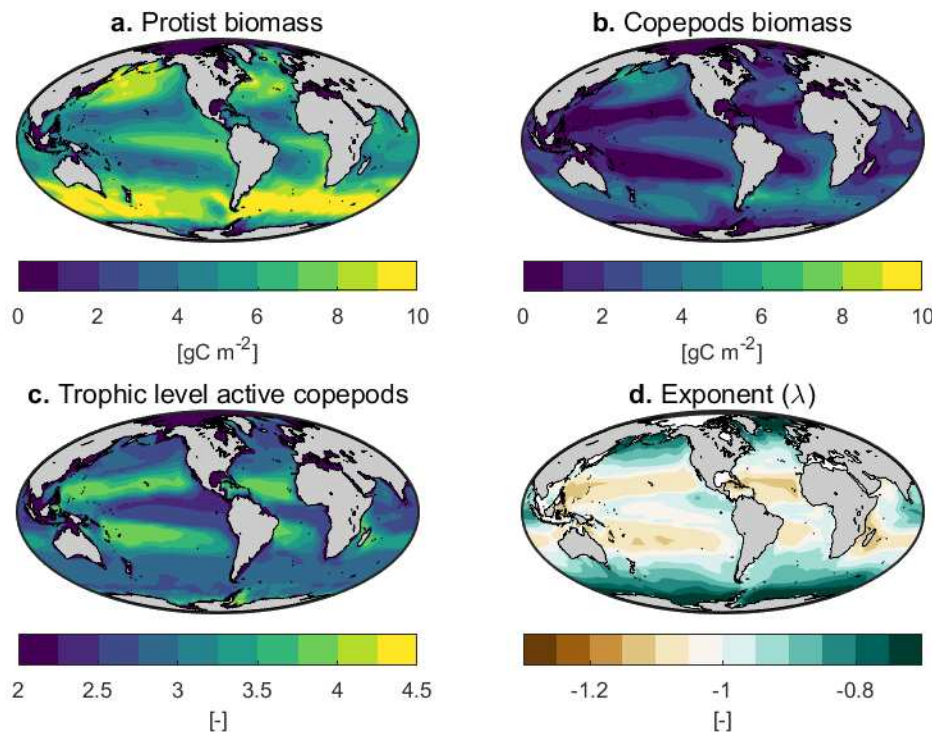


**Figure 2.** Model predictions: yearly averaged biomass of (a) protists and (b) copepods. (c) average trophic level of active copepods averaged over the year (trophic level is calculated as explained in the SI section B). (d) Yearly averaged exponent of the community size-spectrum (see figure D.1 in the SI explaining how we fit the size spectrum and obtain the parameters).

267

### 3.2 Size spectrum

268  
269  
270  
271  
272  
273  
274  
275  
276  
277  
278  
279  
280  
281

The model produces a community size spectrum (Fig. 5). We fitted a power-law function ( $B_{sp} = \kappa m^\lambda$ ) to the normalized community biomass spectrum to obtain the coefficient ( $\kappa$ ) and the exponent ( $\lambda$ ). The yearly averaged exponent varies between  $-1.3$  and  $-0.7$ . The exponent is always negative and always close to the theoretical value of  $-1$  (Andersen & Beyer, 2006). The lowest values (steeper slopes) appear in oligotrophic regions, and the largest values in productive regions (Fig. 2). Exponents obtained from field data are also close to  $-1$  (Fig. 6). Our model fits well data trends at low latitudes, but overestimates the slope at high latitudes. The data yields lower exponents at latitudes close to  $-50$  and  $50$ , particularly during the summer cruises (AMT 12 and 14, Fig. 6a,c). For the southern regions this could again be explained by iron limitation. For the northern regions, a possible reason is the presence of copepods that perform seasonal migrations, which we do not have in the model. In this case, these copepods would be present earlier in the year and deplete the system faster than in our model. In any case, both the data and model show an exponent always close to the theoretical prediction of  $-1$ .

282  
283  
284  
285  
286  
287

Changes in the exponent seem to be driven by the presence/absence of the smallest protists size-classes and the largest copepods (Fig. 5). Some parts of the size spectrum, however, do not fit well a power-law function (e.g. Fig. 5b,c), particularly within the protists size-range. This is due to a plankton bloom, where a specific phytoplankton size group dominates the system. This highlights that a wide range of body-sizes is needed to properly fit a size-spectrum.

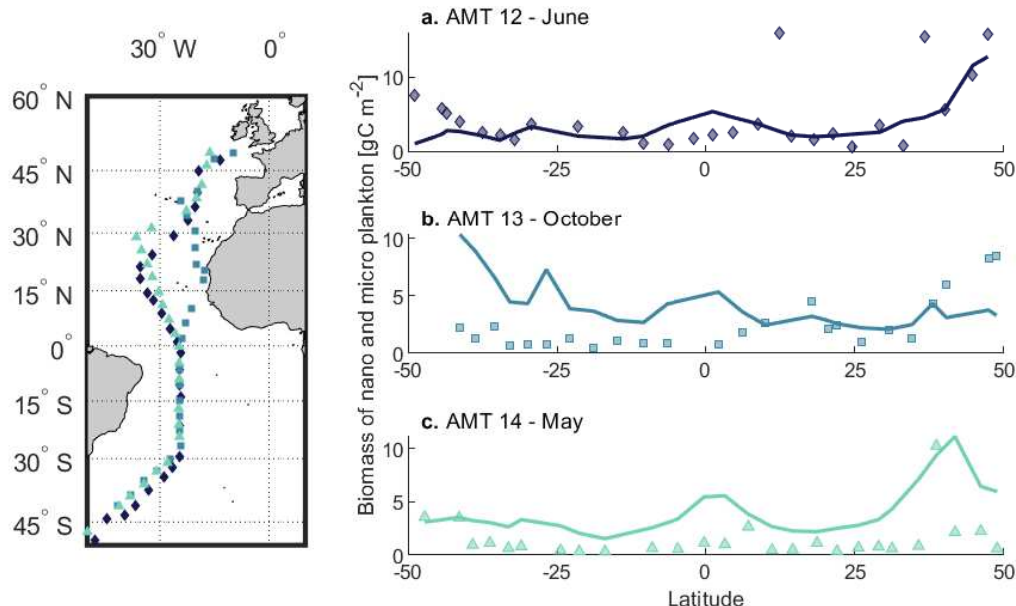


**Figure 3.** Nano- and micro-plankton biomass from the model (continuous lines) versus data (markers), both integrated over the upper 50 m. Biomass data is from three Atlantic Meridional Transects (AMT): (a) AMT 12 (May-June 2003), (b) AMT 13 (September-October 2003), and (c) AMT 14 (April-June 2004). Left panel shows stations where the data was collected. Data extracted from San Martin et al. (2006).

288

### 3.3 Food-web structure and trophic level

289  
290  
291  
292  
293  
294  
295  
296

Food-web structure and trophic levels vary across regions and time (Fig. 2c and 7). The average trophic level of active copepods is highest in oligotrophic regions (Fig. 2c), where it is close to level 4, indicating long food-webs. The biomass of active copepods in these oligotrophic regions is fairly low. In temperate and sub-arctic regions, the average trophic level of active copepods decreases to between 2 and 3 (Fig. 2c and 7). This occurs when the size of primary producers increases (e.g. Fig. 7b,c versus a). Trophic levels close to 2 indicate that copepods feed mostly on primary producers, efficiently transferring energy to large organisms that produce fast-sinking particles.

297  
298  
299  
300  
301  
302

Copepods of different sizes can have similar trophic levels (Fig. 7b,c). Small passive copepods often have the same trophic level as large active copepods. This is due to the lower predator-prey mass ratio of passive feeding copepods relative to active feeders. Hence, communities dominated by passive feeders are less efficient than communities dominated by active feeders at transferring energy to large organisms and exporting carbon.

303

### 3.4 Primary production, carbon flux and export efficiency

304  
305  
306  
307  
308  
309

Yearly averaged NPP is high in temperate and equatorial regions and lowest in the oligotrophic gyres (Fig. 8a). The annual global NPP is  $62 \text{ PgC year}^{-1}$ , within the range of global NPP estimated by remote sensing (between  $36$  and  $78 \text{ PgC year}^{-1}$ , Carr et al., 2006). Compared to field data (Fig. 9), our model performs well in some regions such as the North Atlantic and BATS but does not perform well in the Southern Ocean, where it can underestimate NPP by up to an order of magnitude. This may be due to the coarse

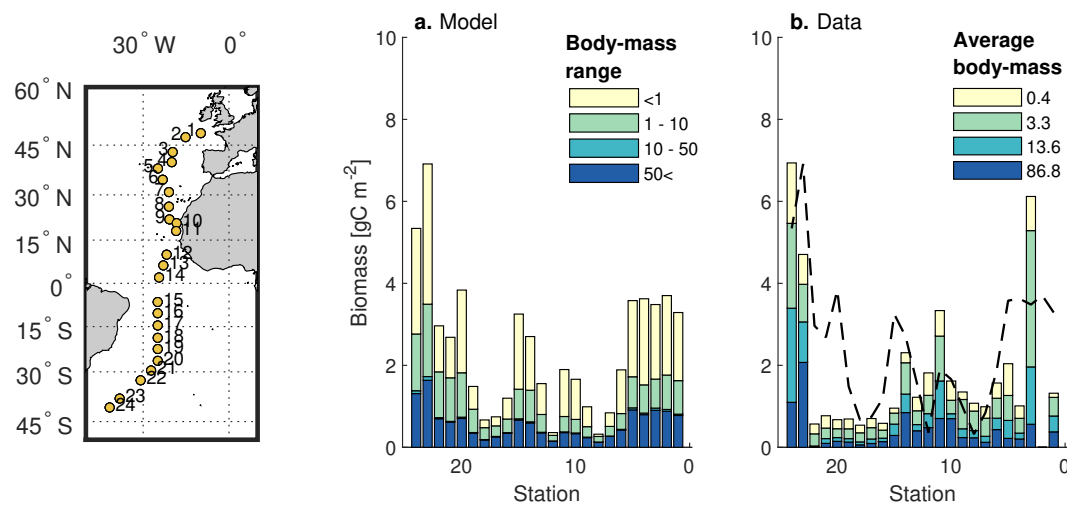


**Figure 4.** Copepod biomass along the Atlantic Meridional Transect for different body-size ranges (September-October). (a) Model estimates. (b) Data from López and Anadón (2008), obtained by multiplying the abundance by the average body-mass within each size range from field data. The smallest size-class combines adult copepods and nauplii. For easier comparison between simulated and observed data, the dashed line in panel b is the total copepod biomass from the model (from panel a). Left panel shows the stations where the data was collected in López and Anadón (2008).

resolution of our physical model, which results in low light levels in the surface layers. Also, NPP data in the Southern Ocean are large and variable, possibly due to some of the data being collected in a frontal zone. Still, the RMSD values in most regions are similar to or lower than the ones obtained from other NPP models (Saba et al., 2011) (note that the comparison might sometimes be imprecise due to data averaging in some bins of the transport matrix).

Global carbon export is  $7.4 \text{ PgC year}^{-1}$  at 120 m (and  $2.0 \text{ PgC year}^{-1}$  at 1080 m), which is within recent estimates of global carbon export ( $6.6 \text{ PgC year}^{-1}$  in Siegel et al. (2014) and  $9.1 \text{ PgC year}^{-1}$  in DeVries and Weber (2017)). Yearly integrated carbon export is highest in tropical and in temperate regions (Fig. 8b and c). Compared to field data of  $^{234}\text{Th}$  measured at depths between 80 and 150 m (Fig. 9b), the spread is rather large. The yearly pe-ratio at 120 m ranges between  $\approx 0$  in oligotrophic regions to more than 0.4 in polar regions, and pe-ratio at 1080 m is below 0.1 in most regions except in polar regions, where it reaches almost 0.2 (Fig. 8d,e).

The composition of the sinking material varies across regions and depth (Fig. 10). Deadfalls dominate export at 120 m in oligotrophic regions, in the North Atlantic, and in the Southern Ocean (Fig. 10a). Elsewhere, deadfalls and copepods fecal pellets contribute similarly to the surface carbon flux (Fig. 10b,c). However, deep export (1080 m), is dominated by fecal pellets produced by large copepods, except in the Southern Ocean and the North Atlantic. In these regions, dead cells still contribute 60% of the deep export. In conclusion, the composition of the carbon export is highly variable close to the surface, but is mainly dominated by large fecal pellets below 1000 m.

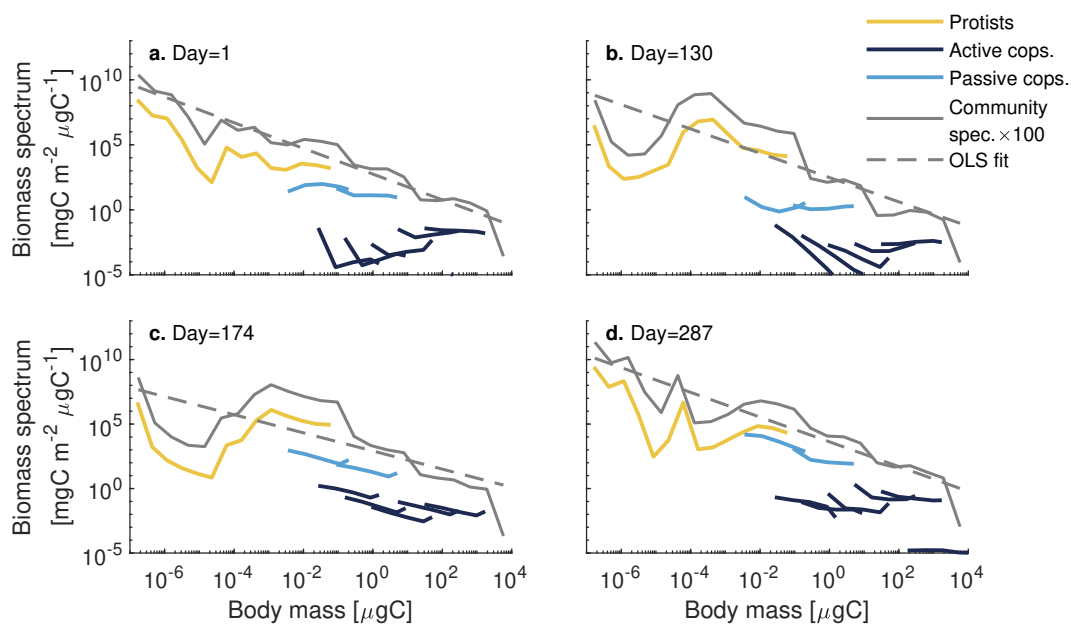


**Figure 5.** Normalized biomass spectra of the community at different times of the year in the North Atlantic: (a) winter, (b) spring, (c) summer, (d) autumn. Protists (yellow), active copepods (dark blue), passive copepods (light blue). Biomass spectra of the community (grey, we multiplied it by 100 for better visualisation), and least square fit (grey dashed line). To calculate the community spectrum, the community was divided into 24 logarithmic evenly distributed mass groups, and therefore the resolution is coarser than the spectrum within each group. The community spectrum does not include detritus.

332

### 3.5 Relation between export, pe-ratio and community metrics

333  
334  
335  
336  
337

To explore the relations between community metrics and carbon export, we performed a correlation analysis of export and pe-ratio at 120 m and 1080 m with the exponent of the size spectrum, the average trophic level of active copepods, and copepod biomass. We also compared the performance of these community metrics with other more commonly used metrics such as NPP and sea surface temperature (SST, Fig. 11).

338  
339  
340  
341  
342  
343

The exponent of the size spectrum correlates strongly with pe-ratio at all depths (Fig. 11k,p), and with surface export (Fig. 11a). Large exponents (“flatter” spectra) result in high and efficient export, whereas low exponents (steeper spectra) result in low and inefficient export. That is because the exponent of the size spectrum provides information on how efficiently energy reaches large organisms that are efficient carbon exporters.

344  
345  
346  
347  
348  
349  
350  
351  
352

Copepod biomass correlates well with carbon export (Fig. 11b,g). This is not surprising, since in the model, copepods produce faster-sinking particles relative to protists. Due to the relative constant size-distribution of copepods, an increase in copepod biomass also incurs an increase in large copepods that contribute the most to deep export. On the other hand, surface pe-ratio is mainly unrelated to copepod biomass (Fig. 11l). In this case, there is a lower bound of copepod biomass until which pe-ratio and copepod biomass are uncorrelated, and after this threshold is surpassed, any kind of pe-ratio can be found. This effect is smoothed for the deep pe-ratio, where there is again a stronger relationship with copepod biomass (Fig. 11q).

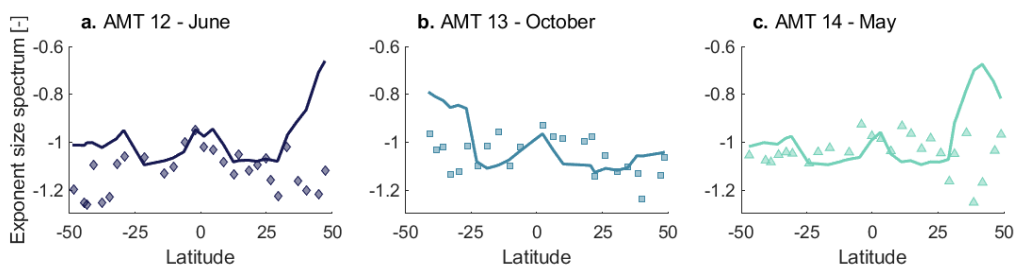


**Figure 6.** Exponent of the size spectrum from the model (continuous lines) and from field samples (markers). Data is from three Atlantic Meridional Transects (AMT): (a) AMT 12 (May-June 2003), (b) AMT 13 (September-October 2003), and (c) AMT 14 (April-June 2004), extracted from San Martin et al. (2006). Stations can be found in figure 3 of this paper.

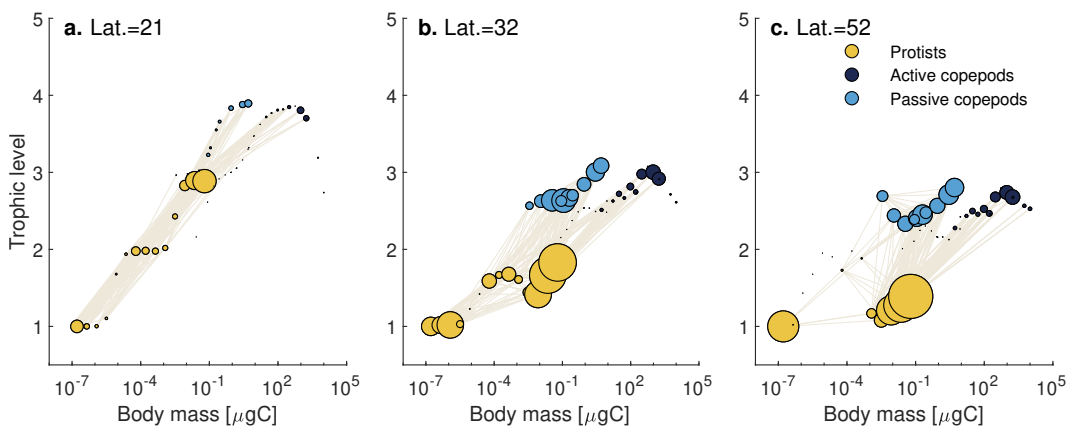


**Figure 7.** Food-webs emerging from the model shown as trophic levels (y-axis) vs. body-mass (x-axis) for three latitudes (21, 32, 52) in the North Pacific. Circle size (area) represents biomass relative to a common value for all panels. Lines connecting circles show the strength of the trophic interaction (i.e. predation, smallest values have been removed for clarity). Trophic level is calculated as explained in SI section B. Decimal trophic levels can occur due to a correction to account for mixotrophy. This also results in some large protists having a lower trophic level than their prey.

353 The average trophic level of active copepods has the strongest (negative) correlation  
 354 with carbon export (Fig. 11c,h). The pe-ratio shows no clear relation with trophic  
 355 level (Fig. 11m,r), similar to the relationship described for copepod biomass.

356 NPP shows two trends with carbon export (Fig. 11d,i), one for low latitudes and  
 357 another for high latitudes. On the other hand, NPP correlates negatively with pe-ratio  
 358 at higher latitudes and has no clear relation at low latitudes (Fig. 11n). The variabil-  
 359 ity increases for both deep export and deep pe-ratio (Fig. 11j,s), weakening the relation-  
 360 ship between the two variables.

361 Finally, temperature shows no clear relation with export (Fig. 11e,j), but is strongly  
 362 related to pe-ratio (Fig. 11o,t).

363 Overall, at the annual level, carbon export correlates best with total copepod biomass  
 364 and the average trophic level of active copepods. On the other hand, pe-ratio correlates

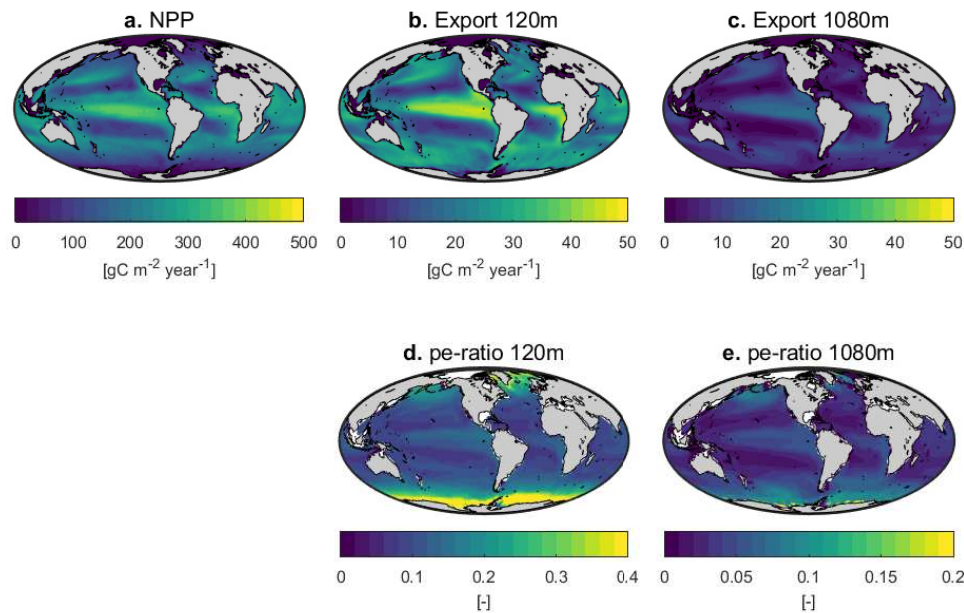


**Figure 8.** Yearly integrated (a) NPP, (b) particle export at 120 m, (c) particle export at 1080 m, (d) pe-ratio at 120 m, (e) pe-ratio at 1080 m.

best with the exponent of the size spectrum and with temperature. Finally, NPP was strongly and negatively related to the surface pe-ratio in productive systems only. For both SST and NPP the effect weakened for deep pe-ratio.

### 3.6 Seasonality and time-lags

Until now we have considered yearly integrated rates. However, the dynamics of export and its efficiency vary over the season. We examine this in three regions with different dynamics: North Pacific, North Atlantic and an oligotrophic gyre. The North Pacific has large copepods throughout the year (Fig. 12d) and a gradual increase of phytoplankton biomass and NPP during spring (Fig. 12g). The North Atlantic has a phytoplankton bloom almost twice as intense as in the North Pacific (Fig. 12h) and copepods appear relatively late in the season (Fig. 12e). Finally, the oligotrophic gyre has a very low copepod biomass and is dominated by a microbial food-web (Fig. 12c,f).

The different dynamics between the North Atlantic and North Pacific emerge from the differences in winter phytoplankton biomass due to deep mixing. In the North Pacific, copepods are sustained by protists biomass during the winter, and are able to control the phytoplankton spring bloom, which is therefore not very pronounced. There is still a time-lag between copepods and protists, but shorter compared to the one in the North Atlantic. The constant presence of large copepods results in carbon export being dominated by fecal pellets, even during the spring bloom. The pe-ratio is high and follows the dynamics of export, particularly just after the bloom when NPP decreases while export is still high.

In the north Atlantic, copepod biomass is lower because copepods need to recover from the deep winter mixing. The delay between the spring bloom and peak biomass is also longer, and therefore most export is dominated by dead protists in spring during

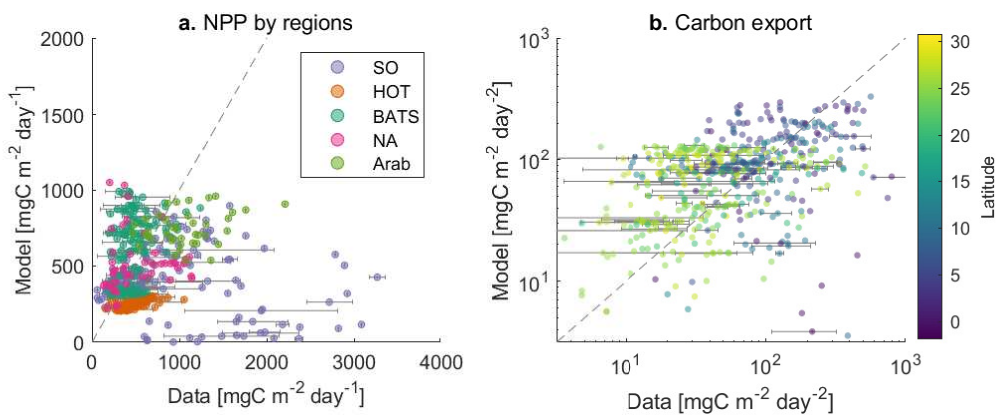


**Figure 9.** Model vs. data of (a) NPP and (b) carbon export. Colors in panel a show different ocean regions: Southern Ocean (SO, RMSD=0.53), Hawaii Ocean Time-series (HOT, RMSD=0.28), Bermuda Atlantic Time-series Study (BATS, RMSD=0.22), eastern North Atlantic (NA, RMSD=0.27), and Arabian Sea (Arab, RMSD=0.20). Colors in panel b represent latitude. Error bars appear for data that fall within the same day and bin in the transport matrix, where the shown data point is the average. NPP data was obtained from the data-set compiled in Saba et al. (2011), and carbon export data from the data-set compiled in Le Moigne et al. (2013), extended in S. Henson et al. (2019). See figures D.2 and D.3 in the Supporting Information for sampling locations.

389 and after the bloom (Fig. 12k). In this case, the pe-ratio at 120 m is very high just af-  
 390 ter the bloom, but is heavily attenuated due to the slower sinking rates and therefore  
 391 does not result in a high pe-ratio at 1000 m. Hence, time-lags affect the composition of  
 392 the export flux, but not necessarily the pe-ratio. Ultimately the pe-ratio is defined by  
 393 total export, the fast dynamics of NPP relative to export (e.g. after the bloom), and com-  
 394 munity composition, the latter defining the sinking rates of particles.

395 The exponent of the size spectrum follows surface pe-ratio trends, but does not nec-  
 396 cessarily follow the trend of deep pe-ratio (Fig. 12p-u). It thus seems that pe-ratio cor-  
 397 relates well with variation of the exponent across regions but not necessarily over time  
 398 within a specific region.

## 399 4 Discussion

400 We sought to understand how carbon export and its efficiency relate to the size spec-  
 401 trum and community composition of the planktonic community. These metrics included  
 402 the exponent of the size spectrum, trophic level of organisms, and copepod biomass. We  
 403 also wanted to understand how time-lags between primary producers and copepods af-  
 404 fected export and its efficiency. The analysis was made with a mechanistic trait-based  
 405 model that resolves the size structure of both the planktonic community and the sink-  
 406 ing detritus. Food web structures and size spectra emerge from the model rather than  
 407 being prescribed. Simulated biomass of copepods and protists follow well-observed trends  
 408 from field data. The emergent food-webs and size-spectra result in differences in carbon  
 409 export and its efficiency.

410 The main results are: (i) carbon export correlates best with copepod biomass and  
 411 the average trophic level of active copepods, whereas (ii) pe-ratio correlates best with  
 412 the exponent of the size spectrum and SST. (iii) These community metrics correlate bet-

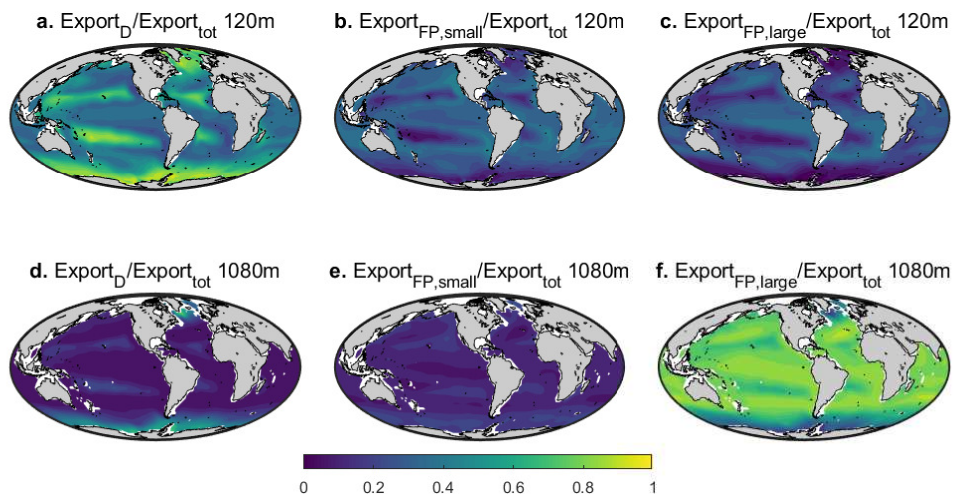


**Figure 10.** Contribution to total export from dead cells (a,d), fecal pellets from small copepods (b,e), and from large copepods(c,f) at 120 m (upper panels) and 1080 m (lower panels). Small copepods are below 1mm.

413 ter with deep export and deep pe-ratio than commonly used metrics, such as NPP or  
 414 SST. Finally, (iv) time-lags between phytoplankton and copepods change the composi-  
 415 tion of the material exported, but do not strongly affect export or pe-ratio.

#### 416 4.1 Can we use size spectra to estimate carbon export and its efficiency?

417 The modelled carbon export correlates better with the exponent of the size spec-  
 418 trum than with NPP or temperature. An interesting avenue could therefore be to use  
 419 this metric to estimate carbon export. However, measuring a size-spectrum in the field  
 420 is not easy, as it requires sampling organisms/particles that range several orders of mag-  
 421 nitude in mass. Therefore, many studies focus on sampling only one part of the size spec-  
 422 trum (e.g. phytoplankton). Dynamics of specific size-groups of unicellular organisms can  
 423 quickly vary in time, for example, during a phytoplankton bloom. In such conditions,  
 424 a power-law will not fit the spectrum when only the phytoplankton size-range is consid-  
 425 ered (Fig. 5b,c). The irregularities observed in size-spectra (often referred as “domes”)  
 426 are common (Sheldon & Parsons, 1967). These domes reflect other properties of the food-  
 427 web, such as changing top- vs. bottom-up control within a size range (Rossberg et al.,  
 428 2019). Thus, size-spectrum theory applies only when fitted across a wide size-range of  
 429 organisms.

430 Field-sampling over a large size range is possible (Lombard et al., 2019), but the  
 431 space and time resolution of these measurements is scarce and the collection demand-  
 432 ing. An approach that would overcome this limitation is to get proxies of the size-spectrum  
 433 via remote sensing (Kostadinov et al., 2009), however this approach still needs to be val-  
 434 idated. If sampling plankton size-spectra in the field becomes easier to achieve, or if good  
 435 proxies of the size-spectrum are developed, size-spectra may become a powerful tool to  
 436 quantify ecosystem processes such as trophic transfer efficiency to large organisms (such  
 437 as fish) and carbon export to the deep ocean.

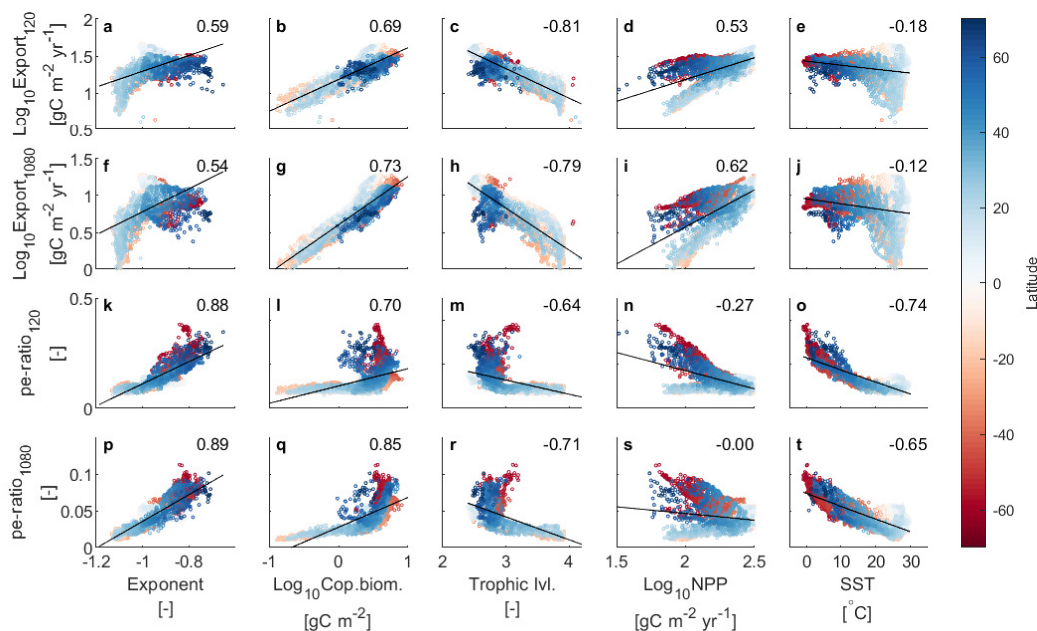


**Figure 11.** Correlation plots for export and pe-ratio at 120 m and 1080 m against the exponent of the size-spectrum (a,f,k,p), copepod biomass (b,g,l,q), average trophic level of active copepods (c,h,m,r), NPP (d,i,n,s), and SST (e,j,o,t). Rates are yearly integrated, the rest is yearly averaged. Numbers in the upper corner of each panel show the Spearman correlation coefficient.

438

## 4.2 Export, pe-ratio, and time-lags

439  
440  
441  
442  
443  
444  
445  
446  
447  
448  
449  
450  
451  
452

Time-lags between primary production and peak copepod biomass do not affect carbon export or its efficiency *per-se*. They mainly affect the composition of the material being exported. Some studies suggest that strong trophic coupling between phytoplankton and their predators can reduce export and its efficiency due to trophic transfer losses and higher remineralization rates in the surface ocean (Parsons, 1988; S. Henson et al., 2019). These studies often assume the predator to be mesozooplankton. However, here, we show that deep export is maximal when copepod biomass is high. Conversely, dominance by protists during spring blooms results in large surface export, but not deep export. We expect this latter result to change if formation of detrital aggregates was modelled. As aggregates become larger, their sinking rates increase. This may particularly happen during diatom blooms, potentially resulting in a high export and pe-ratio in “uncoupled systems”. Overall, whether export and its efficiency are high or low in coupled or uncoupled systems depend on how efficient prey are at exporting carbon relative to their predators.

453  
454  
455  
456  
457  
458  
459  
460

Another result from the model is that surface export often lags NPP, and deep export does not follow NPP dynamics. These differences in timing between export and NPP complicate the interpretation of pe-ratio values. For instance, the pe-ratio at surface follows carbon export, whereas the deep pe-ratio is not necessarily higher when deep export is high. Rather, the deep pe-ratio increases when NPP decreases. These differences in rate of change of export and NPP have been shown to give different pe-ratios depending on how NPP is averaged (Laws & Maiti, 2019). Total export has a more intuitive dynamic than pe-ratio, since pe-ratio is a function of two rates that vary at different time-

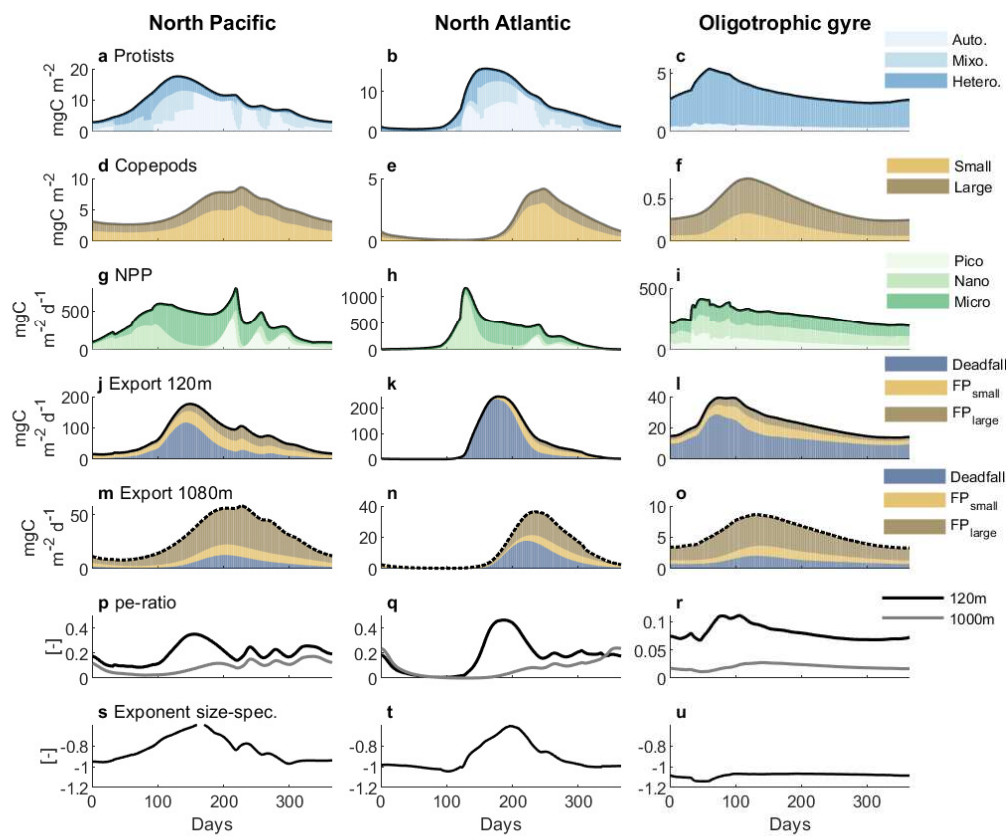


**Figure 12.** Seasonal dynamics in the North Pacific, North Atlantic and an oligotrophic region. (a,b,c) biomass of protists, (d,e,f) biomass of copepods. (g,h,i) NPP, (j-o) export at 120 m and at 1080 m, (p-r) pe-ratio at 120 and 1080 m and (s-u) exponent of the normalized size-spectrum. Note different scales on the y-axis within columns.

461 scales and where the uncertainties of both measurements are propagated. Thus, estimating  
 462 total export may be more useful than attempting to estimate the pe-ratio.

#### 463 4.3 Contribution by copepods to carbon export

464 Deep export in most regions is dominated by fecal pellets of large copepods, even  
 465 in oligotrophic regions. This result agrees with other studies that found copepod size to  
 466 be an important driver of carbon export (Stamieszkin et al., 2015). This is, however, not  
 467 necessarily supported by other studies. Using field data, a recent study found regimes  
 468 of low carbon export in regions where macrozooplankton biomass and bacteria were high  
 469 (S. Henson et al., 2019). Other studies argue that copepods can strongly attenuate the  
 470 carbon flux by fragmenting detrital particles (Wexels Riser et al., 2007, 2010; Cavan et  
 471 al., 2017; Mayor et al., 2020). We consider consumption of detritus by copepods, but not  
 472 a reduction in particle size due to particle fragmentation. Therefore, in the model, losses  
 473 by simple trophic transfer are not enough to attenuate the flux.

474 **4.4 Comparison with other models and model limitations**

475 Our model fits biomass data well, but less so in terms of NPP and carbon export.  
476 Other models which are optimised with observations perform better at estimating these  
477 rates (Stock et al., 2014; Siegel et al., 2014; DeVries & Weber, 2017), but provide less  
478 mechanistic detail. Still, in terms of NPP, the variation found for each region is lower  
479 or similar to the values found in 21 NPP models (Saba et al., 2011), suggesting that the  
480 model performs relatively well. Similarly, our global estimate of carbon export at 100 m,  
481 7.4 PgC year<sup>-1</sup>, falls within the range of estimated values of some of the most recent stud-  
482 ies (6.6 PgC year<sup>-1</sup> in Siegel et al. (2014) and 9.1 PgC year<sup>-1</sup> in DeVries and Weber (2017)).  
483 It should also be kept in mind that the data used to validate models have high uncer-  
484 tainties. We used a global data-set where carbon export by sinking particles was mea-  
485 sured via the <sup>234</sup>Th method. However, due to adsorption of <sup>234</sup>Th on filters and pref-  
486 erential collection of suspended versus sinking particles, this method can underestimate  
487 the carbon flux by approximately 2-fold in some regions (Quay, 1997; Buesseler et al.,  
488 2000). Moreover, the variability of export in each region is high, and often the standard  
489 deviations in each region are close or larger than the mean value (Le Moigne et al., 2013).  
490 Hence, given the uncertainty in NPP and export observations, it is hard to reliably val-  
491 idate model performance.

492 Despite the high ecological complexity of our model, the biogeochemistry is sim-  
493 plistic. We use nitrogen as the sole nutrient in the system, whereas most global mod-  
494 els consider other limiting nutrients such as iron, phosphorus or silica (S. Henson et al.,  
495 2011; DeVries & Weber, 2017; Ward et al., 2018), which can be important limiting fac-  
496 tors in some ocean regions. Therefore the model does not resolve iron limited regions (e.g.  
497 the southern ocean). In addition, the coarse resolution of the transport matrix prevented  
498 us from obtaining carbon export just below the photic layer, which has been recommended  
499 in recent studies (Buesseler et al., 2020). Instead we measured it at fixed depths (120 m  
500 and 1080 m) probably causing some biases when comparing carbon export across regions.

501 Protists in the model are not separated into functional groups. Instead, the trophic  
502 strategy (autotrophy, mixotrophy or heterotrophy) emerges as a function of cell size and  
503 the environment. This configuration still captures the main dynamics observed in na-  
504 ture: a dominance of small primary producers in oligotrophic regions, larger primary pro-  
505 ducers in more productive regions, and the constant presence of unicellular zooplank-  
506 ton and the microbial food-web. This simplification becomes an advantage as it captures  
507 complex dynamics while being based on a relatively low set of parameters and processes.

508 Other organisms that may contribute significantly to carbon export but are not in-  
509 cluded in our model are gelatinous zooplankton (Luo et al., 2020). The inclusion of these  
510 organisms would probably increase export due to (i) their large bodies that can quickly  
511 sink to the bottom, and (ii) their large predator-prey mass ratio. Large predator-prey  
512 mass ratios generate “shortcuts” in the food-web, where energy from very small organ-  
513 isms is efficiently transferred to larger ones, further enhancing carbon export and its ef-  
514 ficiency. Some recent global models now include gelatinous zooplankton (Heneghan et  
515 al., 2020), but these organisms still lack in most (all?) global biogeochemical models.

516 Finally, we do not represent diel and seasonal vertical migrations of zooplankton.  
517 Vertical migration play an important role in the survival and life cycle of copepods, and  
518 in carbon export (Jónasdóttir et al., 2015; Hansen & Visser, 2016; Steinberg & Landry,  
519 2017; Pinti et al., 2021). Implementing vertical migrations may be done through opti-  
520 misation (e.g. Brun et al., 2019; Pinti et al., 2019; Pinti & Visser, 2019). However, im-  
521 plementing behaviour together with population dynamics is challenging, especially if con-  
522 sidered at the global scale. Implementing the active export pathway is urgently needed,  
523 since other modelling studies have suggested that the active carbon flux may have been  
524 responsible for increasing the efficiency of the biological carbon pump (Fakhraee et al.,  
525 2020).

526 **5 Conclusion**

527 We have investigated how carbon export and its efficiency relate to the size spec-  
528 trum and community composition of the planktonic community. We have shown that  
529 carbon export correlates well with copepod biomass and trophic level, and that pe-ratio  
530 correlates best with the exponent of the size spectrum and temperature. Community met-  
531 rics correlate better with deep export and deep pe-ratio than SST and NPP. Time-lags  
532 between phytoplankton and zooplankton do not necessarily affect carbon export or its  
533 efficiency. Our framework captures complex community dynamics scaled from simple individual-  
534 level processes. The model also successfully captures observed inter-biome differences in  
535 plankton biomass and rates. This study has shown the potential of more complex eco-  
536 logical models to explore and understand ecosystem functions and biogeochemical pro-  
537 cesses at the global scale.

538 **Acknowledgments**

539 This work was supported by the Gordon and Betty Moore Foundation through award  
540 5479, and by the Centre for Ocean Life, a VRI Centre for Excellence funded by the Vil-  
541 lum Foundation. CSP was also funded by the Simons Foundation Postdoctoral Fellow-  
542 ship in Marine Microbial Ecology. B.A.W. was funded by a Royal Society University Re-  
543 search Fellowship. Data-sets for this research are included in these papers (and their sup-  
544 plementary information files): San Martin et al. (2006); López and Anadón (2008); Saba  
545 et al. (2011); Le Moigne et al. (2013); S. Henson et al. (2019).

546 **References**

547 Alldredge, A. L., & Gotschalk, C. (1988). In situ settling behavior of marine snow 1.  
548 *Limnology and Oceanography*, 33(3), 339–351. doi: <https://doi.org/10.4319/lo.1988.33.3.0339>

549 Andersen, K. H. (2019). *Fish ecology, evolution, and exploitation: a new theoretical  
550 synthesis*. Princeton University Press. (ISBN: 0691192952, 9780691192956)

551 Andersen, K. H., Berge, T., Gonçalves, R. J., Hartvig, M., Heuschele, J., Hylander,  
552 S., ... others (2016). Characteristic sizes of life in the oceans, from bacteria to  
553 whales. *Annual review of marine science*, 8, 217–241.

554 Andersen, K. H., Beyer, J., & Lundberg, P. (2009). Trophic and individual effi-  
555 cies of size-structured communities. *Proceedings of the Royal Society B: Biolog-  
556 ical Sciences*, 276(1654), 109–114.

557 Andersen, K. H., & Beyer, J. E. (2006). Asymptotic size determines species abun-  
558 dance in the marine size spectrum. *The American Naturalist*, 168(1), 54–61.

559 Bisson, K., Siegel, D. A., & DeVries, T. (2020). Diagnosing mechanisms of ocean  
560 carbon export in a satellite-based food web model. *Frontiers in Marine Sci-  
561 ence*.

562 Brun, P., Stamieszkin, K., Visser, A. W., Licandro, P., Payne, M. R., & Kiørboe,  
563 T. (2019). Climate change has altered zooplankton-fuelled carbon ex-  
564 port in the north atlantic. *Nature ecology & evolution*, 3(3), 416–423. doi:  
565 <https://doi.org/10.1038/s41559-018-0780-3>

566 Buesseler, K. O., Boyd, P. W., Black, E. E., & Siegel, D. A. (2020). Metrics that  
567 matter for assessing the ocean biological carbon pump. *Proceedings of the Na-  
568 tional Academy of Sciences*, 117(18), 9679–9687.

569 Buesseler, K. O., Steinberg, D. K., Michaels, A. F., Johnson, R. J., Andrews, J. E.,  
570 Valdes, J. R., & Price, J. F. (2000). A comparison of the quantity and com-  
571 position of material caught in a neutrally buoyant versus surface-tethered  
572 sediment trap. *Deep Sea Research Part I: Oceanographic Research Papers*,  
573 47(2), 277–294.

574 Carr, M.-E., Friedrichs, M. A., Schmeltz, M., Aita, M. N., Antoine, D., Arrigo,  
575 K. R., ... others (2006). A comparison of global estimates of marine pri-

577 mary production from ocean color. *Deep Sea Research Part II: Topical*  
578 *Studies in Oceanography*, 53(5-7), 741–770. doi: <https://doi.org/10.1016/j.dsr2.2006.01.028>

580 Cavan, E. L., Henson, S. A., Belcher, A., & Sanders, R. (2017). Role of zooplankton  
581 in determining the efficiency of the biological carbon pump. *Biogeosciences*,  
582 14, 177–186. doi: <https://doi.org/10.5194/bg-14-177-2017>

583 Chakraborty, S., Nielsen, L. T., & Andersen, K. H. (2017). Trophic strategies of uni-  
584 cellular plankton. *The American Naturalist*, 189(4), E77–E90. doi: <http://orcid.org/0000-0003-4177-3205>

586 de Roos, A. M., Schellekens, T., Van Kooten, T., Van De Wolfshaar, K., Claessen,  
587 D., & Persson, L. (2008). Simplifying a physiologically structured population  
588 model to a stage-structured biomass model. *Theoretical population biology*,  
589 73(1), 47–62. doi: <https://doi.org/10.1016/j.tpb.2007.09.004>

590 DeVries, T., & Weber, T. (2017). The export and fate of organic matter in  
591 the ocean: New constraints from combining satellite and oceanographic  
592 tracer observations. *Global Biogeochemical Cycles*, 31(3), 535–555. doi:  
593 <https://doi.org/10.1002/2016GB005551>

594 Ducklow, H. W., Steinberg, D. K., & Buesseler, K. O. (2001). Upper ocean carbon  
595 export and the biological pump. *OCEANOGRAPHY-WASHINGTON DC-  
596 OCEANOGRAPHY SOCIETY-*, 14(4), 50–58. doi: <https://doi.org/10.5670/oceanog.2001.06>

598 Dunne, J. P., Armstrong, R. A., Gnanadesikan, A., & Sarmiento, J. L. (2005).  
599 Empirical and mechanistic models for the particle export ratio. *Global Biogeo-  
600 chemical Cycles*, 19(4). doi: <https://doi.org/10.1029/2004GB002390>

601 Dutkiewicz, S., Follows, M. J., & Parekh, P. (2005). Interactions of the iron and  
602 phosphorus cycles: A three-dimensional model study. *Global Biogeochemical  
603 Cycles*, 19(1). doi: <https://doi.org/10.1029/2004GB002342>

604 Fakhraee, M., Planavsky, N. J., & Reinhard, C. T. (2020). The role of environmental  
605 factors in the long-term evolution of the marine biological pump. *Nature Geo-  
606 science*, 13(12), 812–816. doi: <https://doi.org/10.1038/s41561-020-00660-6>

607 Hansen, A. N., & Visser, A. W. (2016). Carbon export by vertically migrating  
608 zooplankton: an optimal behavior model. *Limnology and Oceanography*, 61(2),  
609 701–710. doi: <https://doi.org/10.1002/lno.10249>

610 Hartvig, M., Andersen, K. H., & Beyer, J. E. (2011). Food web framework for size-  
611 structured populations. *Journal of theoretical Biology*, 272(1), 113–122.

612 Heneghan, R. F., Everett, J. D., Sykes, P., Batten, S. D., Edwards, M., Takahashi,  
613 K., ... Richardson, A. J. (2020). A functional size-spectrum model of the  
614 global marine ecosystem that resolves zooplankton composition. *Ecological  
615 Modelling*, 435, 109265. doi: <https://doi.org/10.1016/j.ecolmodel.2020.109265>

616 Henson, S., Le Moigne, F., & Giering, S. (2019). Drivers of carbon export effi-  
617 ciency in the global ocean. *Global Biogeochemical Cycles*, 33(7), 891–903. doi:  
618 <https://doi.org/10.1029/2018GB006158>

619 Henson, S., Sanders, R., Madsen, E., Morris, P. J., Le Moigne, F., & Quartly, G. D.  
620 (2011). A reduced estimate of the strength of the ocean's biological carbon  
621 pump. *Geophysical Research Letters*, 38(4). doi: <https://doi.org/10.1029/2011GL046735>

623 Henson, S. A., Yool, A., & Sanders, R. (2015). Variability in efficiency of particulate  
624 organic carbon export: A model study. *Global Biogeochemical Cycles*, 29(1),  
625 33–45.

626 Jónasdóttir, S. H., Visser, A. W., Richardson, K., & Heath, M. R. (2015). Seasonal  
627 copepod lipid pump promotes carbon sequestration in the deep north atlantic.  
628 *Proceedings of the National Academy of Sciences*, 112(39), 12122–12126. doi:  
629 <https://doi.org/10.1073/pnas.1512110112>

630 Khatiwala, S. (2007). A computational framework for simulation of biogeochemi-  
631 cal tracers in the ocean. *Global Biogeochemical Cycles*, 21(3). doi: <https://doi.org/10.1029/2006GL026207>

632 .org/10.1029/2007GB002923

633 Khatiwala, S., Visbeck, M., & Cane, M. A. (2005). Accelerated simulation of pas-  
634 sive tracers in ocean circulation models. *Ocean Modelling*, 9(1), 51–69. doi:  
635 <https://doi.org/10.1016/j.ocemod.2004.04.002>

636 Kiørboe, T. (2000). Colonization of marine snow aggregates by invertebrate zoo-  
637 plankton: abundance, scaling, and possible role. *Limnology and Oceanography*,  
638 45(2), 479–484. doi: <https://doi.org/10.4319/lo.2000.45.2.0479>

639 Kiørboe, T., & Hirst, A. G. (2014). Shifts in mass scaling of respiration, feeding,  
640 and growth rates across life-form transitions in marine pelagic organisms. *The  
641 American Naturalist*, 183(4), E118–E130.

642 Koski, M., Valencia, B., Newstead, R., & Thiele, C. (2020). The missing piece of the  
643 upper mesopelagic carbon budget? biomass, vertical distribution and feeding  
644 of aggregate-associated copepods at the pap site. *Progress in Oceanography*,  
645 181, 102243. doi: <https://doi.org/10.1016/j.pocean.2019.102243>

646 Kostadinov, T., Siegel, D., & Maritorena, S. (2009). Retrieval of the particle size  
647 distribution from satellite ocean color observations. *Journal of Geophysical Re-  
648 search: Oceans*, 114(C9).

649 Laws, E. A., Falkowski, P. G., Smith Jr, W. O., Ducklow, H., & McCarthy, J. J.  
650 (2000). Temperature effects on export production in the open ocean. *Global  
651 Biogeochemical Cycles*, 14(4), 1231–1246. doi: <https://doi.org/10.1029/1999GB001229>

652 Laws, E. A., & Maiti, K. (2019). The relationship between primary production and  
653 export production in the ocean: Effects of time lags and temporal variability.  
654 *Deep Sea Research Part I: Oceanographic Research Papers*, 148, 100–107. doi:  
655 <https://doi.org/10.1016/j.dsr.2019.05.006>

656 Le Moigne, F., Henson, S., Sanders, R., & Madsen, E. (2013). Global database  
657 of surface ocean particulate organic carbon export fluxes diagnosed from  
658 the 234th technique. *Earth System Science Data*, 5(2), 295–304. doi:  
659 <https://doi.org/10.5194/essd-5-295-2013>

660 Lombard, F., Boss, E., Waite, A. M., Vogt, M., Uitz, J., Stemmann, L., . . . others  
661 (2019). Globally consistent quantitative observations of planktonic ecosystems.  
662 *Frontiers in Marine Science*, 6, 196.

663 Longhurst, A. R., & Harrison, W. G. (1989). The biological pump: profiles of plank-  
664 ton production and consumption in the upper ocean. *Progress in Oceanogra-  
665 phy*, 22(1), 47–123.

666 López, E., & Anadón, R. (2008). Copepod communities along an atlantic merid-  
667 ional transect: Abundance, size structure, and grazing rates. *Deep Sea  
668 Research Part I: Oceanographic Research Papers*, 55(10), 1375–1391. doi:  
669 [https://doi.org/10.1016/0079-6611\(89\)90010-4](https://doi.org/10.1016/0079-6611(89)90010-4)

670 Luo, J. Y., Condon, R. H., Stock, C. A., Duarte, C. M., Lucas, C. H., Pitt, K. A., &  
671 Cowen, R. K. (2020). Gelatinous zooplankton-mediated carbon flows in the  
672 global oceans: A data-driven modeling study. *Global Biogeochemical Cycles*,  
673 34(9), e2020GB006704. doi: <https://doi.org/10.1029/2020GB006704>

674 Mayor, D. J., Gentleman, W. C., & Anderson, T. R. (2020). Ocean carbon se-  
675 questration: Particle fragmentation by copepods as a significant unrecognised  
676 factor? explicitly representing the role of copepods in biogeochemical models  
677 may fundamentally improve understanding of future ocean carbon storage.  
678 *BioEssays*, 42(12), 2000149. doi: <https://doi.org/10.1002/bies.202000149>

679 McNair, H. M., Morison, F., Graff, J. R., Rynearson, T. A., & Menden-Deuer, S.  
680 (2021). Microzooplankton grazing constrains pathways of carbon export in the  
681 subarctic north pacific. *Limnology and Oceanography*.

682 Parsons, T. R. (1988). Trophodynamic phasing in theoretical, experimental and  
683 natural pelagic ecosystems. *Journal of the Oceanographical Society of Japan*,  
684 44(2), 94–101. doi: <https://doi.org/10.1007/BF02303124>

685 Pinti, J., Andersen, K. H., & Visser, A. W. (2021). Co-adaptive behavior of inter-

687 acting populations in a habitat selection game significantly impacts ecosystem  
688 functions. *Journal of Theoretical Biology*, 523, 110663.

689 Pinti, J., Kiørboe, T., Thygesen, U. H., & Visser, A. W. (2019). Trophic interactions  
690 drive the emergence of diel vertical migration patterns: a game-theoretic  
691 model of copepod communities. *Proceedings of the Royal Society B*, 286(1911),  
692 20191645. doi: <https://doi.org/10.1098/rspb.2019.1645>

693 Pinti, J., & Visser, A. W. (2019). Predator-prey games in multiple habitats reveal  
694 mixed strategies in diel vertical migration. *The American Naturalist*, 193(3),  
695 E65–E77.

696 Quay, P. (1997). Was a carbon balance measured in the equatorial pacific during  
697 jgofs? *Deep Sea Research Part II: Topical Studies in Oceanography*, 44(9-10),  
698 1765–1781.

699 Rossberg, A. G., Gaedke, U., & Kratina, P. (2019). Dome patterns in pelagic size  
700 spectra reveal strong trophic cascades. *Nature communications*, 10(1), 1–11.

701 Saba, V. S., Friedrichs, M. A., Antoine, D., Armstrong, R., Asanuma, I., Behrenfeld, M., ... others (2011). An evaluation of ocean color model estimates of  
702 marine primary productivity in coastal and pelagic regions across the globe.  
703 *Biogeosciences*, 489–503. doi: <https://doi.org/10.5194/bg-8-489-2011>

704 San Martin, E., Harris, R. P., & Irigoien, X. (2006). Latitudinal variation in plankton size spectra in the atlantic ocean. *Deep Sea Research Part II: Topical Studies in Oceanography*, 53(14-16), 1560–1572. doi: <https://doi.org/10.1016/j.dsr2.2006.05.006>

705 Serra-Pompei, C., Soudijn, F., Visser, A. W., Kiørboe, T., & Andersen, K. H.  
706 (2020). A general size-and trait-based model of plankton communities.  
707 *Progress in Oceanography*, 102473. doi: <https://doi.org/10.1016/j.pocean.2020.102473>

708 Sheldon, R., & Parsons, T. (1967). A continuous size spectrum for particulate matter in the sea. *Journal of the Fisheries Board of Canada*, 24(5), 909–915.

709 Siegel, D., Buesseler, K., Doney, S., Sailley, S., Behrenfeld, M. J., & Boyd, P. (2014).  
710 Global assessment of ocean carbon export by combining satellite observations  
711 and food-web models. *Global Biogeochemical Cycles*, 28(3), 181–196.

712 Small, L., Fowler, S., & Ünlü, M. (1979). Sinking rates of natural copepod fecal pellets.  
713 *Marine Biology*, 51(3), 233–241. doi: <https://doi.org/10.1007/BF00386803>

714 Sprules, W. G., & Barth, L. E. (2016). Surfing the biomass size spectrum: some  
715 remarks on history, theory, and application. *Canadian Journal of Fisheries and  
716 Aquatic Sciences*, 73(4), 477–495. doi: <https://doi.org/10.1139/cjfas-2015-0115>

717 Sprules, W. G., & Munawar, M. (1986). Plankton size spectra in relation to ecosystem  
718 productivity, size, and perturbation. *Canadian Journal of Fisheries and  
719 Aquatic Sciences*, 43(9), 1789–1794. doi: <https://doi.org/10.1139/f86-222>

720 Stamieszkin, K., Pershing, A. J., Record, N. R., Pilskaln, C. H., Dam, H. G., &  
721 Feinberg, L. R. (2015). Size as the master trait in modeled copepod fecal  
722 pellet carbon flux. *Limnology and Oceanography*, 60(6), 2090–2107. doi:  
723 <https://doi.org/10.1002/lno.10156>

724 Steinberg, D. K., & Landry, M. R. (2017). Zooplankton and the ocean carbon cycle.  
725 *Annual Review of Marine Science*, 9, 413–444. doi: <https://doi.org/10.1146/annurev-marine-010814-015924>

726 Stock, C., Dunne, J., & John, J. (2014). Drivers of trophic amplification of ocean  
727 productivity trends in a changing climate. *Biogeosciences Discussions*, 11(7).  
728 doi: <https://doi.org/10.5194/bg-11-7125-2014>

729 Ward, B. A., & Follows, M. J. (2016). Marine mixotrophy increases trophic transfer  
730 efficiency, mean organism size, and vertical carbon flux. *Proceedings of the National  
731 Academy of Sciences*, 113(11), 2958–2963.

732 Ward, B. A., Wilson, J. D., Death, R. M., Monteiro, F. M., Yool, A., & Ridgwell,  
733

742 A. (2018). Ecogenie 1.0: plankton ecology in the cgenie earth system model.  
743 *Geoscientific Model Development*, 11(10), 4241–4267.

744 Wassmann, P. (1997). Retention versus export food chains: processes controlling  
745 sinking loss from marine pelagic systems. *Hydrobiologia*, 363(1-3), 29–57.

746 Wexels Riser, C., Reigstad, M., & Wassmann, P. (2010). Zooplankton-mediated car-  
747 bon export: A seasonal study in a northern norwegian fjord. *Marine Biology*  
748 *Research*, 6(5), 461–471. doi: <https://doi.org/10.1080/17451000903437067>

749 Wexels Riser, C., Reigstad, M., Wassmann, P., Arashkevich, E., & Falk-Petersen, S.  
750 (2007). Export or retention? copepod abundance, faecal pellet production and  
751 vertical flux in the marginal ice zone through snap shots from the northern  
752 barents sea. *Polar Biology*, 30(6), 719–730. doi: <https://doi.org/10.1007/s00300-006-0229-z>

753

754 \*References from main text and SI combined